

## DIFFRACTION OF NONLINEAR RANDOM WAVES BY A VERTICAL CYLINDER IN DEEP WATER

A. KAREEM,\* A. N. WILLIAMS† and C. C. HSIEH‡

\*Department of Civil Engineering and Geological Science, University of Notre Dame, Notre Dame, IN 46556-0767, U.S.A.; †Department of Civil and Environmental Engineering, University of Houston, Houston, TX 77204-4791, U.S.A.

**Abstract**—A solution, exact to second-order, is presented for the nonlinear diffraction of random waves by a fixed, surface-piercing vertical circular cylinder in deep water. The incident wave field is considered as a stationary random process, and the nonlinear diffraction problem is analyzed utilizing the Stokes perturbation expansion procedure combined with a Fourier–Stieltjes spectral representation of the stationary random wave kinematics. The second-order velocity potential is explicitly obtained by applying a modified form of Weber’s Integral Theorem to invert the inhomogeneous second-order free-surface condition. Particular attention is directed towards the second-order diffraction forces on the cylinder. The spectral description of the second-order diffraction forces involves a complicated integral expression with highly oscillatory wave–wave interaction kernels and multiple convolutions of the linear wave spectrum. The present approach provides a complete spectral description of the second-order diffraction forces, and yields the spectral densities of the diffraction forces at the sum and difference frequencies. Numerical results are presented which illustrate the spectral content of the diffraction force due to an incident wave field represented by a superposition of waves described by band-limited white noise processes centered at different frequencies.

### INTRODUCTION

THE ESTIMATION of wave diffraction loading on fixed, vertical surface-piercing cylinders has been a subject under investigation for decades ever since the analysis of the diffraction of linear waves in infinite water depth was reported by Havelock (1940). MacCamy and Fuchs (1954) subsequently extended this theory for the case of finite water depth. However, the results of the linear diffraction theory are based on linearized conditions on the free-surface, and therefore its application is restricted to waves of small amplitude. For waves of finite amplitude, a diffraction theory which is able to account for free-surface nonlinearities in a consistent manner is necessary.

Nonlinear diffraction analyses that involve the extension of the linear theory of Havelock or MacCamy and Fuchs to include finite wave amplitude effects resulting from the diffraction of second-order Stokes waves have been reported by several investigators. The main difficulty in formulating a consistent second-order diffraction theory has been in the correct treatment of the inhomogeneous free-surface boundary condition which appears at second-order and, consequently, several incomplete solutions exist in the literature [see, for example, Williams (1989) for a review].

In view of the difficulties associated with specifying a complete form for the second-order potential, in recent years much attention has been focused on an indirect approach, originally due to Molin (1979) and Lighthill (1979), in which the second-order hydrodynamic loads may be calculated without the explicit calculation of the

second-order potential. Examples of the use of this technique may be found in the works of Eatock Taylor and Hung (1987), Abul-Azm and Williams (1988, 1989a, b) and Ghalayini and Williams (1989, 1991). Also, most recently, numerical schemes based on the source-sink technique (integral equation approach) utilizing appropriate Green's functions have been utilized to obtain second-order diffraction loads and local quantities such as the second-order wave elevation and pressure distribution. Examples of these methods, for both monochromatic and bichromatic incident waves, may be found in the papers of Kim and Yue (1989, 1990, 1991), Kim (1991) and Eatock Taylor and Chau (1992).

In the present paper the nonlinear diffraction of deepwater random waves by a vertical circular cylinder to second-order is investigated. This is in contrast to the above works which treated monochromatic or bichromatic wave diffraction only. In general, physical quantities of a random wave field can be represented by Fourier-Stieltjes spectral integrals (Doob, 1953; Yaglom, 1962) provided that the random wave field is statistically stationary in time and homogeneous in space. The method employed herein is a direct solution for the second-order velocity potential, formulated in terms of Fourier-Bessel integrals (Hunt and Baddour, 1981; Hunt and Williams, 1982) and inverted by means of a modified form of Weber's Integral Theorem (Griffith, 1956, 1957). Subsequently, explicit expressions for the nonlinear diffraction loading (up to second-order) on the cylinder in the direction of wave propagation are developed. In particular, the mean and power spectral density of the nonlinear diffraction loads are evaluated. The numerical results illustrate that the spectral density of the second-order diffraction forces may be significant at both low and high frequencies.

#### FORMULATION

A fixed, surface-piercing, vertical circular cylinder of radius  $a$  is subjected to unidirectional random waves in deep water. The flow is assumed irrotational and the fluid incompressible. Hence, the fluid motion may be characterized by a velocity potential  $\Phi$  and the fluid velocity vector is given by  $\mathbf{q} = \nabla\Phi$ . The velocity potential  $\Phi$  satisfies Laplace's equation,

$$\nabla^2\Phi(r,\theta,z,t) = 0, \quad (1)$$

where  $t$  denotes time. A cylindrical coordinate system  $(r,\theta,z)$  is employed with the  $z$ -axis directed upwards from an origin at the mean water level which coincides with the axis of the cylinder (see Fig. 1). The fluid is also subjected to the following boundary conditions:

$$\Phi_z \rightarrow 0 \quad \text{as } z \rightarrow -\infty, \quad (2)$$

$$\Phi_r = 0 \quad \text{at } r = a \quad -\infty < z < \eta, \quad (3)$$

$$\eta_t + \Phi_r \eta_r + \frac{1}{r^2} \Phi_\theta \eta_\theta - \Phi_z = 0 \quad \text{at } z = \eta, \quad \text{and} \quad (4)$$

$$\Phi_t + \frac{1}{2} \left[ \Phi_r^2 + \left( \frac{1}{r} \Phi_\theta \right)^2 + \Phi_z^2 \right] + g\eta = 0 \quad \text{at } z = \eta, \quad (5)$$

where  $\eta(r,\theta,t)$  denotes the free-surface elevation,  $g$  is the acceleration due to gravity and subscripts indicate partial differentiation.

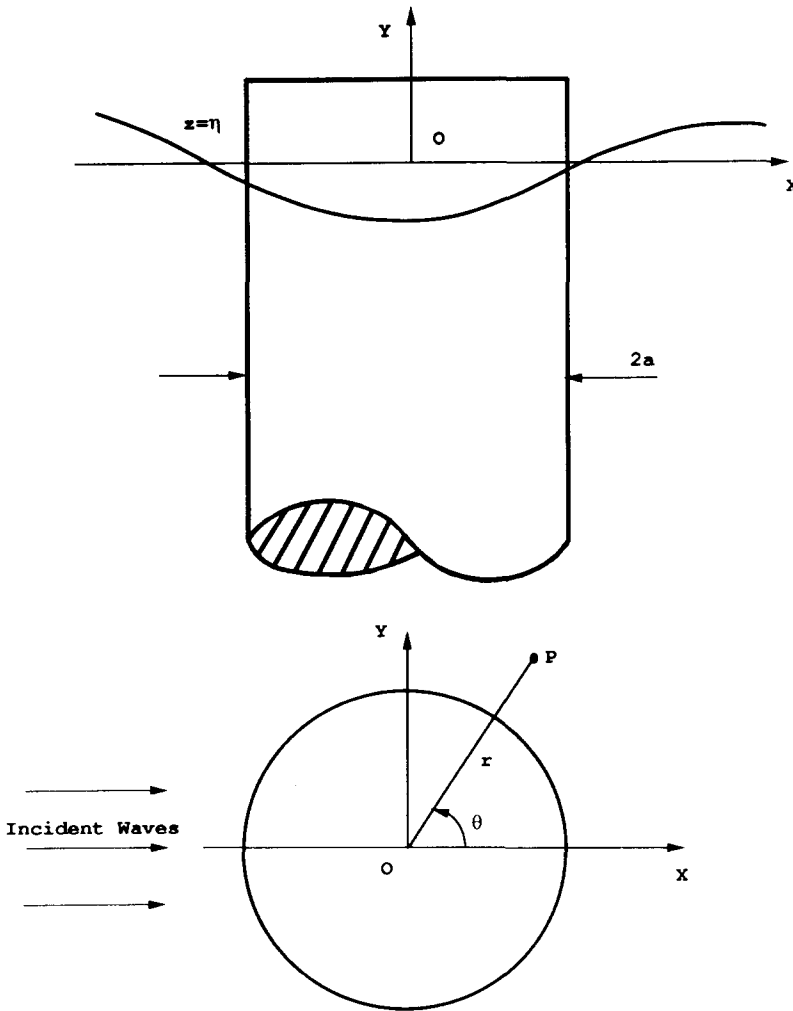


FIG. 1. Definition sketch for a vertical circular cylinder subjected to unidirectional random waves in deep water.

The velocity potential  $\Phi$  and the free surface elevation  $\eta$  are expressed in Stokes perturbation expansions as

$$\Phi = \epsilon\Phi^{(1)} + \epsilon^2\Phi^{(2)} + \dots \tag{6}$$

$$\eta = \epsilon\eta^{(1)} + \epsilon^2\eta^{(2)} + \dots, \tag{7}$$

where  $\Phi^{(j)}$  and  $\eta^{(j)}$ ,  $j = 1, 2, \dots$  do not functionally depend on the perturbation parameter  $\epsilon$ , which physically represents an averaged wave steepness, and  $\epsilon$  is assumed sufficiently small such that the convergence of the power series solutions is ensured.

Expanding the nonlinear free-surface boundary conditions, Equations (4) and (5), in Taylor series about  $z = 0$ , substituting the Stokes perturbation series in Equations

(6) and (7) for  $\Phi$  and  $\eta$ , and equating terms in like powers of  $\varepsilon$ , leads to boundary conditions at various orders in  $\varepsilon$  at  $z = 0$ , valid for all  $r$ ,  $\theta$  and  $t$ . Therefore, for the first-order, the boundary conditions at  $z = 0$  are

$$\eta_t^{(1)} - \Phi_z^{(1)} = 0, \quad (8)$$

$$\mathbf{g}\eta^{(1)} + \Phi_r^{(1)} = 0, \quad (9)$$

and, at second-order,

$$\eta_t^{(2)} - \Phi_z^{(2)} = \Phi_r^{(1)}\eta_r^{(1)} - \frac{1}{r^2}\Phi_\theta^{(1)}\eta_\theta^{(1)} + \eta^{(1)}\Phi_{zz}^{(1)}, \quad (10)$$

$$\mathbf{g}\eta^{(2)} + \Phi_r^{(2)} = \eta^{(1)}\Phi_{rz}^{(1)} - \frac{1}{2}\left\{[\Phi_r^{(1)}]^2 + \left[\frac{1}{r}\Phi_\theta^{(1)}\right]^2\right\}. \quad (11)$$

For convenience,  $\eta^{(1)}$  and  $\eta^{(2)}$  are usually eliminated to give boundary conditions on  $\Phi^{(1)}$  and  $\Phi^{(2)}$  alone, namely

$$\Phi_{rr}^{(1)} + \mathbf{g}\Phi_z^{(1)} = 0, \quad (12)$$

$$\Phi_{rr}^{(2)} + \mathbf{g}\Phi_z^{(2)} = \frac{1}{\mathbf{g}}\Phi_{tt}^{(1)}\frac{\partial}{\partial z}[\Phi_{rr}^{(1)} + \mathbf{g}\Phi_z^{(1)}] - \frac{\partial}{\partial t}\left\{[\Phi_r^{(1)}]^2 + [\Phi_z^{(1)}]^2 + \left[\frac{1}{r}\Phi_\theta^{(1)}\right]^2\right\}. \quad (13)$$

Also, Equations (1)–(3) may be rewritten in terms of the first-order and second-order velocity potentials as

$$\nabla^2\Phi^{(1)} = 0, \quad \nabla^2\Phi^{(2)} = 0, \quad (14)$$

$$\Phi_z^{(1)} \rightarrow 0, \quad \Phi_z^{(2)} \rightarrow 0 \quad \text{as } z \rightarrow -\infty, \quad (15)$$

$$\Phi_r^{(1)} = 0, \quad \Phi_r^{(2)} = 0 \quad \text{at } r = a. \quad (16)$$

There remain two further conditions to be satisfied by  $\Phi^{(1)}$  and  $\Phi^{(2)}$ , namely radiation conditions as  $r$  tends to infinity. These prove not to be the same. The condition on  $\Phi^{(1)}$  will be addressed in the first-order solution and the condition on  $\Phi^{(2)}$  cannot be assigned before the first-order solution is developed.

#### FIRST-ORDER SOLUTION

The first-order diffraction theory for random waves in the presence of a vertical circular cylinder in deep water may be obtained in a way similar to that applied by MacCamy and Fuchs (1954). The first-order velocity potential is considered to be composed of incident and scattered components, namely

$$\Phi^{(1)} = \Phi_I^{(1)} + \Phi_S^{(1)}, \quad (17)$$

where the incident velocity potential,  $\Phi_I^{(1)}$ , represents a random wave field in which waves propagate unidirectionally (in the  $x$ -direction). According to the spectral representation theorem for stationary random processes (Doob, 1953; Yaglom, 1962), the incident wave field can be expressed as

$$\Phi_I^{(1)}(x, z, t) = \int_{-\infty}^{\infty} -\frac{i\mathbf{g}}{\omega} e^{\omega^2 z/\mathbf{g}} e^{i(|\omega|x/\mathbf{g} - \omega t)} d\xi(\omega), \quad (18)$$

where  $\xi(\omega)$  is a random process with uncorrelated increments,  $d\xi(\omega)$ , satisfying the following

$$E[d\xi(\omega)] = 0 \tag{19a}$$

in which  $S_{\eta\eta}(\omega)$  denotes the incident wave spectrum (two-sided),  $\omega$  is the circular frequency in rad/sec, the symbol \* denotes the complex conjugate. It is noted that  $d\xi^*(\omega) = d\xi(-\omega)$  is required to make  $\Phi_I^{(1)}$  real valued. Moreover, since  $d\xi(\omega)$  represents a random wave amplitude of linear waves, it is assumed to be Gaussian. In cylindrical coordinates the incident velocity potential can be written as

$$\begin{aligned} \Phi_I^{(1)}(r, \theta, z, t) = & \int_0^\infty -\frac{i\mathbf{g}}{\omega} \left[ \sum_{n=-\infty}^\infty i^n J_n(\omega^2 r/\mathbf{g}) e^{in\theta} \right] e^{\omega^2 z/\mathbf{g}} e^{-i\omega t} d\xi(\omega) \\ & + \int_{-\infty}^0 -\frac{i\mathbf{g}}{\omega} \left[ \sum_{n=-\infty}^\infty (-i)^n J_n(\omega^2 r/\mathbf{g}) e^{in\theta} \right] e^{\omega^2 z/\mathbf{g}} e^{-i\omega t} d\xi(\omega), \end{aligned} \tag{20}$$

where  $J_n(\cdot)$  denotes the Bessel function of the first kind of order  $n$  and use has been made of the identity,

$$e^{ibx} = e^{ib(r\cos\theta)} = \sum_{n=-\infty}^\infty i^n J_n(br) e^{in\theta}. \tag{21}$$

The corresponding scattered velocity potential is given by

$$\Phi_s^{(1)}(r, \theta, z, t) = \int_{-\infty}^\infty e^{i\Omega t} d\zeta_s(\Omega; r, \theta, z) \tag{22}$$

where  $\zeta_s(\Omega; r, \theta, z)$  denotes a random process with uncorrelated increments,  $d\zeta_s(\Omega; r, \theta, z)$ . Since the scattered velocity potential is required to satisfy Equations (14) and (15), by a separation of variables,  $d\zeta_s(\Omega; r, \theta, z)$  can be written as

$$d\zeta_s(\Omega; r, \theta, z) = \Gamma(r, \theta, k) e^{|k|z} d\xi_s(\Omega), \tag{23}$$

where  $k$  is the separation constant,  $\xi_s(\Omega)$  denotes a random process with uncorrelated increments,  $d\xi_s(\Omega)$ , and  $\Gamma(r, \theta, k)$  is a deterministic function satisfying the Helmholtz equation, namely

$$\Gamma_{rr} + \frac{1}{r} \Gamma_r + \frac{1}{r^2} \Gamma_{\theta\theta} + |k|^2 \Gamma = 0, \tag{24}$$

to which the general solution is given by

$$\Gamma(r, \theta, k) = \sum_{n=-\infty}^\infty [A_n H_n^{(1)}(|k|r) + B_n H_n^{(2)}(|k|r)] e^{in\theta}, \tag{25}$$

where  $H_n^{(1)}(\cdot)$  and  $H_n^{(2)}(\cdot)$  are Hankel functions of the first and second kinds of order  $n$ , and  $A_n$  and  $B_n$  are constants to be determined.

Therefore, the scattered velocity potential can be written as follows:

$$\Phi_s^{(1)}(r, \theta, z, t) = \int_{-\infty}^{\infty} \sum_{n=-\infty}^{\infty} [A_n H_n^{(1)}(|k|r) + B_n H_n^{(2)}(|k|r)] e^{in\theta} e^{|k|z} e^{i\Omega t} d\xi_s(\Omega). \quad (26)$$

Substitution of this form for the scattered potential into the free-surface boundary condition, Equation (12), yields

$$\int_{-\infty}^{\infty} (-\Omega^2 + g|k|) \sum_{n=-\infty}^{\infty} [A_n H_n^{(1)}(|k|r) + B_n H_n^{(2)}(|k|r)] \cdot e^{in\theta} e^{|k|z} e^{i\Omega t} d\xi_s(\Omega) = 0 \quad (27)$$

which implies that

$$-\Omega^2 + g|k| = 0, \quad (28)$$

which is the well-known linear dispersion relation in deep waters. Consequently,  $\Phi_s^{(1)}$  can be expressed as

$$\Phi_s^{(1)}(r, \theta, z, t) = \int_{-\infty}^{\infty} \sum_{n=-\infty}^{\infty} [A_n H_n^{(1)}(\Omega^2 r/g) + B_n H_n^{(2)}(\Omega^2 r/g)] e^{in\theta} e^{\Omega^2 z/g} e^{i\Omega t} d\xi_s(\Omega). \quad (29)$$

As  $\Phi_s^{(1)}$  has to satisfy the radiation condition as  $r \rightarrow \infty$ , terms such as  $H_n^{(1)}(\Omega^2 r/g) e^{i\Omega t}$  for  $\Omega > 0$  and  $H_n^{(2)}(\Omega^2 r/g) e^{i\Omega t}$  for  $\Omega < 0$ , which represent waves propagating from infinity toward the cylinder, are unacceptable on physical grounds. Thus, the scattered velocity potential can be expressed by

$$\Phi_s^{(1)}(r, \theta, z, t) = \int_0^{\infty} \left[ \sum_{n=-\infty}^{\infty} B_n H_n^{(2)}(\Omega^2 r/g) e^{in\theta} \right] e^{\Omega^2 z/g} e^{i\Omega t} d\xi_s(\Omega) + \int_{-\infty}^0 \sum_{n=-\infty}^{\infty} A_n H_n^{(1)}(\Omega^2 r/g) e^{in\theta} e^{\Omega^2 z/g} e^{i\Omega t} d\xi_s(\Omega). \quad (30)$$

The final condition which  $\Phi_s^{(1)}$  is required to satisfy is the no-flow condition on the cylinder surface, namely

$$\frac{\partial \Phi_s^{(1)}}{\partial r} = -\frac{\partial \Phi_I^{(1)}}{\partial r} \quad \text{on } r = a. \quad (31)$$

From Equations (20) and (30), one may obtain on  $r = a$

$$\frac{\partial \Phi_s^{(1)}}{\partial r} = \int_0^{\infty} \frac{\Omega^2}{g} \sum_{n=-\infty}^{\infty} B_n H_n^{(2)'}(\Omega^2 a/g) e^{in\theta} e^{\Omega^2 z/g} e^{i\Omega t} d\xi_s(\Omega) + \int_{-\infty}^0 \frac{\Omega^2}{g} \sum_{n=-\infty}^{\infty} A_n H_n^{(1)'}(\Omega^2 a/g) e^{in\theta} e^{\Omega^2 z/g} e^{i\Omega t} d\xi_s(\Omega) \quad (32)$$

and

$$\begin{aligned} \frac{\partial \Phi_I^{(1)}}{\partial r} = & - \int_0^\infty i\omega \sum_{n=-\infty}^\infty i^n J_n'(\omega^2 a/g) e^{in\theta} e^{\omega^2 z/g} e^{-i\omega t} d\xi(\omega) \\ & - \int_{-\infty}^0 i\omega \sum_{n=-\infty}^\infty (-i)^n J_n'(\omega^2 a/g) e^{in\theta} e^{\omega^2 z/g} e^{-i\omega t} d\xi(\omega), \end{aligned} \quad (33)$$

where the primes indicate differentiations taken with respect to the arguments. It follows from Equation (31) and temporal equivalence in Equations (32) and (33), that

$$\Omega = -\omega, \quad (34a)$$

and, so

$$d\xi_s(\Omega) = d\xi(-\omega). \quad (34b)$$

Also, the coefficients  $A_n$  and  $B_n$  are given by

$$A_n = \frac{\mathbf{g} i^{n+1} J_n'(\omega^2 a/g)}{\omega H_n^{(1)'}(\omega^2 a/g)}. \quad (35)$$

Consequently,  $\Phi^{(1)}$  can be expressed as

$$\begin{aligned} \Phi^{(1)} = & \int_{-\infty}^\infty \frac{\mathbf{g}}{\omega} \left\{ \sum_{n=-\infty}^\infty \text{sgn}(\omega) [i \text{sgn}(\omega)]^n M_n(\omega^2 a/g) C_n(\omega^2 r/g) e^{i \text{sgn}(\omega) \alpha_n(\omega)} \cdot e^{in\theta} \right\} \\ & e^{\omega^2 z/g} e^{-i\omega t} d\xi(\omega), \end{aligned} \quad (36)$$

where  $\text{sgn}(\cdot)$  denotes the sign function,

$$\begin{aligned} M_n(\omega^2 a/g) &= [J_n'(\omega^2 a/g)^2 + Y_n'(\omega^2 a/g)^2]^{-1/2}, \\ \alpha_n(\omega) &= \tan^{-1} \left[ \frac{Y_n'(\omega^2 a/g)}{J_n'(\omega^2 a/g)} \right] \quad \text{and} \\ C_n(\omega^2 r/g) &= Y_n'(\omega^2 a/g) J_n(\omega^2 r/g) - J_n'(\omega^2 a/g) Y_n(\omega^2 r/g) \quad \text{for } n \geq 0. \end{aligned} \quad (37)$$

For  $n < 0$ , the following relationships may be used:

$$M_n(\cdot) = (-1)^n M_{-n}(\cdot), \quad \alpha_n(\cdot) = \alpha_{-n}(\cdot) \quad \text{and} \quad C_n(\cdot) = C_{-n}(\cdot). \quad (38)$$

From Equation (9), the free-surface elevation on the cylinder surface may be expressed by

$$\begin{aligned} \eta^{(1)}(a, \theta, t) = & \int_{-\infty}^\infty i \left\{ \sum_{n=-\infty}^\infty \text{sgn}(\omega) [i \text{sgn}(\omega)]^n M_n(\omega^2 a/g) C_n(\omega^2 a/g) e^{-i[\text{sgn}(\omega) \alpha_n(\omega)]} \cdot e^{in\theta} \right\} \\ & e^{\omega^2 z/g} e^{-i\omega t} d\xi(\omega). \end{aligned} \quad (39)$$

This expression will subsequently be required in the development of the second-order diffraction force.

SECOND-ORDER SOLUTION

Before determining  $\Phi^{(2)}$ , it is desirable to simplify Equation (13) by utilizing the expression for  $\Phi^{(1)}$ . For deep water, the first term on the right-hand side of Equation (13) is identical to zero as Equation (12) is satisfied for all values of  $z$ , not only for  $z = 0$ . Substituting  $\Phi^{(1)}$  as given in Equation (36) into Equation (13) leads to

$$\Phi_u^{(2)} + \mathbf{g} \Phi_z^{(2)} = \int_{-\infty}^{\infty} \int_{-\infty}^{\infty} \sum_{n=-\infty}^{\infty} \sum_{m=-\infty}^{\infty} f_{n,m}(\omega, \bar{\omega}, r) e^{in\theta} e^{-i(\omega + \bar{\omega})t} d\xi(\omega) d\xi(\bar{\omega}), \tag{40}$$

in which

$$f_{n,m}(\omega, \bar{\omega}, r) = i^{n+1}(\omega + \bar{\omega}) \omega \bar{\omega} \operatorname{sgn}(\omega)^{m+1} \operatorname{sgn}(\bar{\omega})^{n-m+1} \cdot M_m(\omega^2 a/g) M_{n-m}(\bar{\omega}^2 a/g) e^{i[\operatorname{sgn}(\omega)\alpha_m(\omega) + \operatorname{sgn}(\bar{\omega})\alpha_{n-m}(\bar{\omega})]} \cdot \left\{ C'_m(k_1 r) C'_{n-m}(k_2 r) - \frac{m(n-m)}{k_1 k_2 r^2} C_m(k_1 r) C_{n-m}(k_2 r) + C_m(k_1 r) C_{n-m}(k_2 r) \right\}. \tag{41}$$

The second-order velocity potential,  $\Phi^{(2)}$ , may be considered to consist of a homogeneous solution, which satisfies the homogeneous form of Equation (40), and a particular solution. In view of the boundary condition Equation (15), the deepwater homogeneous solution admits no radial evanescent modes, and so can be represented by outwardly propagating waves only. This fact suggests that in the present case the homogeneous and particular solutions may be treated together. Therefore, the total second-order velocity potential is expressed as the following Fourier–Bessel integral:

$$\Phi^{(2)}(r, \theta, z, t) = \int_{-\infty}^{\infty} \int_{-\infty}^{\infty} \sum_{n=-\infty}^{\infty} \sum_{m=-\infty}^{\infty} A_{n,m}(\Omega, k) C_n(kr) e^{|k|z} e^{in\theta} e^{i\Omega t} dk d\xi_2(\Omega), \tag{42}$$

in which  $\Omega$  is the circular frequency,  $\xi_2(\Omega)$  is a random process with uncorrelated increments,  $d\xi_2(\Omega)$ ,  $A_{n,m}(\Omega, k)$  denote unknown coefficients and  $C_n(kr)$  is a cylinder function, given by

$$C_n(kr) = Y'_n(ka)J_n(kr) - J'_n(ka)Y_n(kr). \tag{43}$$

Alternatively,  $\Phi^{(2)}$  can be rewritten as

$$\Phi^{(2)}(r, \theta, z, t) = \int_{-\infty}^{\infty} \int_0^{\infty} \sum_{n=-\infty}^{\infty} \sum_{m=-\infty}^{\infty} G_{n,m}(\Omega, k) C_n(kr) \cdot e^{kz} e^{in\theta} e^{i\Omega t} dk d\xi_2(\Omega), \tag{44}$$

in which the  $G_{n,m}(\Omega, k)$  [which may be related to the  $A_{n,m}(\Omega, k)$ ], are coefficients to be determined and use has been made of the identity,  $C_n(-kr) = -C_n(kr)$  for  $k > 0$ . It can be shown (see Appendix) that  $\Phi^{(2)}$  in this form satisfies Equations (14)–(16).

Substituting  $\Phi^{(2)}$  from Equation (44) into the left-hand side of Equation (13) leads to

$$\Phi_{tt}^{(2)} + \mathbf{g} \Phi_z^{(2)} = \int_{-\infty}^{\infty} \int_0^{\infty} \sum_{n=-\infty}^{\infty} \sum_{m=-\infty}^{\infty} (-\Omega^2 + \mathbf{g}k) G_{n,m}(\Omega, k) C_n(kr) \cdot e^{in\theta} e^{i\Omega t} dk d\xi_2(\Omega). \quad (45)$$

Comparing Equation (45) to Equation (40), it follows from temporal equivalence that

$$\Omega = -(\omega + \bar{\omega}), \quad (46)$$

and, therefore, one obtains

$$d\xi_2(\Omega) = d\xi(\omega) d\xi(\bar{\omega}) \quad (47)$$

and

$$\begin{aligned} f_{n,m}(\omega, \bar{\omega}, r) &= \int_0^{\infty} [\mathbf{g}k - \Omega^2] G_{n,m}(\Omega, k) C_n(kr) dk \\ &= \int_0^{\infty} [\mathbf{g}k - (\omega + \bar{\omega})^2] G_{n,m}(\omega, \bar{\omega}, k) C_n(kr) dk. \end{aligned} \quad (48)$$

In a manner similar to Hunt and Baddour (1981) and Hunt and Williams (1982), the coefficients  $G_{n,m}(\omega, \bar{\omega}, k)$  in Equation (48) may be determined using a modified form of Weber's Integral Theorem, according to which any function  $f(r)$ , satisfying certain conditions (Griffith, 1956, 1957), can be expressed as

$$f(r) = \int_0^{\infty} \frac{C_n(kr)}{[J'_n(ka)^2 + Y'_n(ka)^2]} k dk \int_a^{\infty} C_n(ku) u f(u) du. \quad (49)$$

The solution to Equation (48) is therefore formally

$$G_{n,m}(\omega, \bar{\omega}, k) = \frac{k \int_a^{\infty} C_n(kr) r f_{n,m}(\omega, \bar{\omega}, r) dr}{[\mathbf{g}k - (\omega + \bar{\omega})^2] [J'_n(ka)^2 + Y'_n(ka)^2]}. \quad (50)$$

Utilizing Equations (46) and (47),  $\Phi^{(2)}$  in Equation (44) can thus be rewritten as

$$\begin{aligned} \Phi^{(2)} &= \int_{-\infty}^{\infty} \int_{-\infty}^{\infty} \sum_{n=-\infty}^{\infty} \sum_{m=-\infty}^{\infty} \int_0^{\infty} G_{n,m}(\omega, \bar{\omega}, k) C_n(kr) \\ &\cdot e^{kz} dk e^{in\theta} e^{-i(\omega + \bar{\omega})t} d\xi(\omega) d\xi(\bar{\omega}). \end{aligned} \quad (51)$$

The integral in Equation (50) may be explicitly determined using Equation (41). Integrating by parts and employing Bessel's equation, leads to

$$\begin{aligned} \int_a^{\infty} C_n(kr) r f_{n,m}(\omega, \bar{\omega}, r) dr &= \frac{\beta_{n,m}(\omega, \bar{\omega}, a) [(k_1 + k_2)^2 - k^2]}{2 k_1 k_2} \\ &\cdot \int_a^{\infty} C_n(kr) C_m(k_1 r) C_{n+m}(k_2 r) r dr, \end{aligned} \quad (52)$$

where  $\beta_{n,m}(\omega, \bar{\omega}, a)$  denotes the  $r$ -independent component of  $f_{n,m}(\omega, \bar{\omega}, r)$ . If interest is focused on the diffraction forces in the  $x$ -direction (along  $\theta = 0$ ), then it is necessary to compute  $G_{n,m}(\omega, \bar{\omega}, k)$  for  $n = -1$  and  $1$  only (Hunt and Baddour, 1981; Hunt and Williams, 1982).

### NONLINEAR DIFFRACTION LOADING

The total diffraction load on the cylinder results from the net effect of the fluid pressure over the entire wetted surface of the cylinder. The pressure at any point in a fluid of density  $\rho$  is given, to the second-order, as

$$p = -\varepsilon\rho\Phi_t^{(1)} - \varepsilon^2\rho\left\{\Phi_t^{(2)} + \frac{1}{2}[\nabla\Phi^{(1)}]^2\right\} - \rho g z, \quad (53)$$

and the diffraction force on the cylinder in the  $x$ -direction is

$$F_x(t) = a \int_0^{2\pi} \int_{-\infty}^{\eta} [p]_{r=a} \cos(\pi - \theta) dz d\theta. \quad (54)$$

The diffraction force can be formally expressed as a sum of the first-order and second-order parts, namely

$$F_x(t) = \varepsilon F_x^{(1)}(t) + \varepsilon^2 F_x^{(2)}(t), \quad (55)$$

where

$$F_x^{(1)}(t) = -a\rho \int_0^{2\pi} \int_{-\infty}^0 [\Phi_t^{(1)}]_{r=a} \cos(\pi - \theta) dz d\theta \quad (56)$$

and

$$F_x^{(2)}(t) = -a\rho \int_0^{2\pi} \left\{ \int_0^{\eta^{(1)}} [\Phi_t^{(1)} + g z] dz + \int_{-\infty}^0 \left[ \Phi_t^{(2)} + \frac{1}{2}(\Phi_z^{(1)})^2 + \frac{1}{2a^2}(\Phi_\theta^{(1)})^2 \right] dz \right\}_{r=a} \cos(\pi - \theta) d\theta. \quad (57)$$

Substituting for  $\Phi^{(1)}$ ,  $\eta^{(1)}$  and  $\Phi^{(2)}$  from Equations (37), (39) and (51) into Equations (56) and (57), and carrying out the  $z$ -integrations and  $\theta$ -integrations analytically, leads to

$$F_x^{(1)}(t) = 2a\rho\pi g^2 \int_{-\infty}^{\infty} \omega^{-2} M_1(\omega^2 a/g) C_1(\omega^2 a/g) e^{-i\text{sgn}(\omega)\alpha_1(\omega)} e^{-i\omega t} d\xi(\omega), \quad (58)$$

$$F_x^{(2)}(t) = \frac{a\rho\pi g}{2} \int_{-\infty}^{\infty} \int_{-\infty}^{\infty} \sum_{\substack{n=-1 \\ (n \neq 0)}}^1 \sum_{m=-\infty}^{\infty} \left\{ \chi_{n,m}(\omega, \bar{\omega}, a) \left[ 1 + \frac{\omega\bar{\omega}}{(\omega^2 + \bar{\omega}^2)} - \frac{m(n-m)g^2}{a^2\omega\bar{\omega}(\omega^2 + \bar{\omega}^2)} \right] - \int_0^{\infty} \frac{4i(\omega + \bar{\omega})}{agk^2} G_{n,m}(\omega, \bar{\omega}, k) dk \right\} e^{-i(\omega + \bar{\omega})t} d\xi(\omega) d\xi(\bar{\omega}), \quad (59)$$

where use has been made of the identity,  $C_n(ka) = 2/\pi ka$ , and

$$\chi_{n,m}(\omega, \bar{\omega}, a) = \frac{4g^2}{\pi^2 a^2 \omega \bar{\omega} (\omega + \bar{\omega})} \beta_{n,m}(\omega, \bar{\omega}, a). \quad (60)$$

For convenience, the second-order diffraction loading in Equation (59) is rewritten as

$$F_x^{(2)}(t) = \frac{a\rho\pi g}{2} \int_{-\infty}^{\infty} \int_{-\infty}^{\infty} \sum_{q=0}^{\infty} [K_q(\omega, \bar{\omega}, a) - L_q(\omega, \bar{\omega}, a)] \cdot e^{-i(\omega + \bar{\omega})t} d\xi(\omega) d\xi(\bar{\omega}), \quad (61)$$

where

$$K_q(\omega, \bar{\omega}, a) = 2i[-\text{sgn}(\omega)\text{sgn}(\bar{\omega})]^q \left( \frac{2g}{a\pi\omega\bar{\omega}} \right)^2 \left[ 1 + \frac{\omega\bar{\omega}}{(\omega^2 + \bar{\omega}^2)} + \frac{q(q+1)g^2}{a^2\omega\bar{\omega}(\omega^2 + \bar{\omega}^2)} \right] \cdot \{ \text{sgn}(\omega) M_q(\omega^2 a/g) M_{q+1}(\bar{\omega}^2 a/g) e^{-i[\text{sgn}(\omega)\alpha_q(\omega) + \text{sgn}(\bar{\omega})\alpha_{q+1}(\bar{\omega})]} + \text{sgn}(\bar{\omega}) M_{q+1}(\omega^2 a/g) M_q(\bar{\omega}^2 a/g) e^{-i[\text{sgn}(\omega)\alpha_{q+1}(\omega) + \text{sgn}(\bar{\omega})\alpha_q(\bar{\omega})]} \} \quad (62a)$$

$$L_q(\omega, \bar{\omega}, a) = \int_0^{\infty} \frac{8i(\omega + \bar{\omega})}{agk\pi[ak - (\omega + \bar{\omega})^2][J_1'(ka)^2 + Y_1'(ka)^2]} \left\{ \int_a^{\infty} C_1(kr)[f_{1,-q}(\omega, \bar{\omega}, r) + f_{1,q+1}(\omega, \bar{\omega}, r)] r dr \right\} dk. \quad (62b)$$

It is noted that the wave-wave interaction kernels  $K_q(\dots)$  and  $L_q(\dots)$  depend on the wave frequencies, but not on the wave amplitudes. The term  $L_q(\dots)$  essentially results from the second-order velocity potential, and

$$K_q(\bar{\omega}, \omega, a) = K_q(\omega, \bar{\omega}, a), \quad L_q(\bar{\omega}, \omega, a) = L_q(\omega, \bar{\omega}, a), \\ K_q(-\omega, \omega, a) = K_q(\omega, -\omega, a) \quad \text{and} \quad L_q(\omega, -\omega, a) = L_q(-\omega, \omega, a) = 0. \quad (63)$$

As the nonlinear diffraction force from Equations (55), (58) and (61) is a random quantity, it is appropriate to study its statistical and spectral content. The mean of the nonlinear diffraction force may be expressed as

$$E[F_x(t)] = E[F_x^{(1)}(t) + F_x^{(2)}(t)] \\ = 2a\rho\pi g^2 \int_{-\infty}^{\infty} \omega^{-2} M_1(\omega^2 a/g) C_1(\omega^2 a/g) e^{-i\text{sgn}(\omega)\alpha_1(\omega)} e^{-i\omega t} E[d\xi(\omega)] \\ + \frac{a\rho\pi g}{2} \int_{-\infty}^{\infty} \int_{-\infty}^{\infty} \sum_{q=0}^{\infty} [K_q(\omega, \bar{\omega}, a) - L_q(\omega, \bar{\omega}, a)] e^{-i(\omega + \bar{\omega})t} E[d\xi(\omega) d\xi(\bar{\omega})]. \quad (64)$$

Invoking the probabilistic characteristics of  $\xi(\omega)$  described in the first-order solution and the identities in Equation (63), then Equation (64) becomes

$$\begin{aligned} E[F_x(t)] &= E[F_x^{(2)}(t)] \\ &= a\rho\pi\mathbf{g} \int_0^\infty \sum_{q=0}^\infty K_q(\omega, -\omega, a) S_{\eta\eta}(\omega) d\omega \\ &= -\frac{8\rho\mathbf{g}^3}{a\pi} \int_0^\infty \sum_{q=0}^\infty \frac{\left[1 - \frac{q(q+1)\mathbf{g}^2}{a^2\omega^4}\right] [J'_q Y'_{q+1} - J'_{q+1} Y'_q]}{\omega^4 [J_q'^2 + Y_q'^2] [J_{q+1}'^2 + Y_{q+1}'^2]} S_{\eta\eta}(\omega) d\omega, \quad (65) \end{aligned}$$

where the arguments of the Bessel functions are  $\omega^2 a/\mathbf{g}$ , and  $S_{\eta\eta}(\omega)$  denotes the incident wave spectrum (two-sided). It is noted that the mean of the nonlinear diffraction loading represents the drift force, and it is independent of the second-order velocity potential. The covariance of  $F_x(t)$  is defined as

$$\begin{aligned} \text{cov}[F_x(t), F_x(t+\tau)] &= E\{F_x^{(1)}(t) + F_x^{(2)}(t) [F_x^{(1)}(t+\tau) + F_x^{(2)}(t+\tau)]\} - E^2\{F_x(t)\} \\ &= E\{F_x^{(1)}(t)F_x^{(1)}(t+\tau)\} + E\{F_x^{(1)}(t)F_x^{(2)}(t+\tau) + F_x^{(2)}(t)F_x^{(1)}(t+\tau)\} \\ &\quad + E\{F_x^{(2)}(t)F_x^{(2)}(t+\tau)\} - E^2\{F_x^{(2)}(t)\}. \quad (66) \end{aligned}$$

The first expectation term in Equation (66) is given by

$$\begin{aligned} R_{F_x^{(1)}F_x^{(1)}}(\tau) &= (2a\mathbf{g}^2\rho\pi)^2 \int_{-\infty}^\infty \int_{-\infty}^\infty (\omega\bar{\omega})^{-2} M_1(\omega^2 a/\mathbf{g}) M_1(\bar{\omega}^2 a/\mathbf{g}) C_1(\omega^2 a/\mathbf{g}) C_1(\bar{\omega}^2 a/\mathbf{g}) \\ &\quad \cdot e^{-i[\text{sgn}(\omega)\alpha_1(\omega) + \text{sgn}(\bar{\omega})\alpha_1(\bar{\omega}) + \omega t + \bar{\omega}t + \bar{\omega}\tau]} E[d\xi(\omega) d\xi(\bar{\omega})] \\ &= (2a\mathbf{g}^2\rho\pi)^2 \int_{-\infty}^\infty \frac{M_1(\omega^2 a/\mathbf{g}) C_1(\omega^2 a/\mathbf{g})}{\omega^4} e^{i\omega\tau} S_{\eta\eta}(\omega) d\omega \\ &= 16\rho^2\mathbf{g}^6 \int_{-\infty}^\infty \omega^{-8} [J_1'(\omega^2 a/\mathbf{g})^2 + Y_1'(\omega^2 a/\mathbf{g})^2]^{-1} e^{i\omega\tau} S_{\eta\eta}(\omega) d\omega \quad (67) \end{aligned}$$

in which  $R_{F_x^{(1)}F_x^{(1)}}(\tau) = E\{F_x^{(1)}(t)F_x^{(1)}(t+\tau)\}$  and represents autocorrelation of  $F_x^{(1)}(t)$  force. The second expectation term in Equation (66) is identically zero since the product of the first-order and second-order forces includes a third-order joint moment of Gaussian random variables, that is,  $d\xi(\omega_1) d\xi(\omega_2) d\xi(\omega_3)$ . A combination of the third and fourth terms in Equation (66) gives the covariance of the second-order diffraction forces, namely

$$\text{cov}[F_x^{(2)}(t), F_x^{(2)}(t+\tau)] = R_{F_x^{(2)}F_x^{(2)}}(\tau) - E^2[F_x^{(2)}(t)]. \quad (68)$$

Since an expression for  $E[F_x^{(2)}(t)]$  has been given in Equation (65), and

$$\begin{aligned}
 R_{F_x^{(2)} F_x^{(2)}}(\tau) = & \left( \frac{a g \rho \pi}{2} \right)^2 \int_{-\infty}^{\infty} \sum_{m=0}^{\infty} \sum_{n=0}^{\infty} [K_m(\omega_1, \omega_2, a) K_n(\omega_3, \omega_4, a) \\
 & - K_m(\omega_1, \omega_2, a) L_n(\omega_1, \omega_2, a) - L_m(\omega_1, \omega_2, a) K_n(\omega_3, \omega_4, a) \\
 & + L_m(\omega_1, \omega_2, a) L_n(\omega_1, \omega_2, a)] e^{-i[(\omega_1 + \omega_2 + \omega_3 + \omega_4)t + (\omega_3 + \omega_4)\tau]} \\
 & \cdot E[d\xi(\omega_1) d\xi(\omega_2) d\xi(\omega_3) d\xi(\omega_4)], \quad (69)
 \end{aligned}$$

it follows, after substituting for  $E[d\xi(\omega_1) d\xi(\omega_2) d\xi(\omega_3) d\xi(\omega_4)]$  in terms of lower-order joint moments, that

$$\begin{aligned}
 \text{cov}[F_x^{(2)}(t), F_x^{(2)}(t+\tau)] = & \left( \frac{a g \rho \pi}{2} \right)^2 \int_{-\infty}^{\infty} \int_{-\infty}^{\infty} \sum_{m=0}^{\infty} \sum_{n=0}^{\infty} [K_m(\omega, \lambda - \omega, a) K_n(-\omega, \omega - \lambda, a) \\
 & + K_m(\omega, \lambda - \omega, a) K_n(\omega - \lambda, -\omega, a) - K_m(\omega, \lambda - \omega, a) L_n(-\omega, \omega - \lambda, a) \\
 & - K_m(\omega, \lambda - \omega, a) L_n(\omega - \lambda, -\omega, a) - L_m(\omega, \lambda - \omega, a) K_n(-\omega, \omega - \lambda, a) \\
 & - L_m(\omega, \lambda - \omega, a) K_n(\omega - \lambda, -\omega, a) + L_m(\omega, \lambda - \omega, a) L_n(-\omega, \omega - \lambda, a) \\
 & + L_m(\omega, \lambda - \omega, a) L_n(\omega - \lambda, -\omega, a)] e^{i\lambda\tau} S_{\eta\eta}(\omega) S_{\eta\eta}(\lambda - \omega) d\omega d\lambda. \quad (70)
 \end{aligned}$$

From Equations (66) and (68), the covariance of the nonlinear diffraction force  $F_x(t)$  can be expressed symbolically as

$$\text{cov}[F_x(t), F_x(t+\tau)] = \text{cov}[F_x^{(1)}(t), F_x^{(1)}(t+\tau)] + \text{cov}[F_x^{(2)}(t), F_x^{(2)}(t+\tau)]. \quad (71)$$

The corresponding power spectral density, which can be derived through the Wiener–Khinchine relation, is given by

$$S_{F_x F_x}(\lambda) = S_{F_x^{(1)} F_x^{(1)}}(\lambda) + S_{F_x^{(2)} F_x^{(2)}}(\lambda), \quad (72)$$

where

$$S_{F_x^{(1)} F_x^{(1)}}(\lambda) = \frac{16 \rho^2 g^6 S_{\eta\eta}(\lambda)}{\lambda^8 [J_1'(\lambda^2 a/g)^2 + Y_1'(\lambda^2 a/g)^2]} \quad (73)$$

and

$$\begin{aligned}
 S_{F_x^{(2)} F_x^{(2)}}(\lambda) = & \left( \frac{a g \rho \pi}{2} \right)^2 \int_{-\infty}^{\infty} \sum_{m=0}^{\infty} \sum_{n=0}^{\infty} [K_m(\omega, \lambda - \omega, a) K_n(-\omega, \omega - \lambda, a) \\
 & + K_m(\omega, \lambda - \omega, a) K_n(\omega - \lambda, -\omega, a) - K_m(\omega, \lambda - \omega, a) L_n(-\omega, \omega - \lambda, a) \\
 & - K_m(\omega, \lambda - \omega, a) L_n(\omega - \lambda, -\omega, a) - L_m(\omega, \lambda - \omega, a) K_n(-\omega, \omega - \lambda, a) \\
 & - L_m(\omega, \lambda - \omega, a) K_n(\omega - \lambda, -\omega, a) + L_m(\omega, \lambda - \omega, a) L_n(-\omega, \omega - \lambda, a) \\
 & + L_m(\omega, \lambda - \omega, a) L_n(\omega - \lambda, -\omega, a)] S_{\eta\eta}(\omega) S_{\eta\eta}(\lambda - \omega) d\omega. \quad (74)
 \end{aligned}$$

Subsequently, the standard deviation of  $F_x(t)$  can be readily obtained from the following expression:

$$\begin{aligned} \sigma_F^2 &= \int_{-\infty}^{\infty} S_{F_x F_x}(\lambda) d\lambda \\ &= \int_{-\infty}^{\infty} S_{F_x^{(1)} F_x^{(1)}}(\lambda) d\lambda + \int_{-\infty}^{\infty} S_{F_x^{(2)} F_x^{(2)}}(\lambda) d\lambda. \end{aligned} \tag{75}$$

COMPUTATIONAL CONSIDERATIONS

In the above, the first-order solution presents no computational difficulty whereas the second-order solutions require significant computational effort. As shown in Equation (74), the power spectral density of the second-order diffraction loading involves a complicated multiple convolution integral of the incident wave spectrum and highly oscillatory wave-wave interaction kernels. Numerical methods are utilized to evaluate this integral. One approach is to approximate the incident wave spectrum by band-limited white noise with appropriately determined amplitude at various discrete frequencies that may practically represent the dominant wave components of a random wave field. As such, the continuous incident wave spectrum may then be visualized as composed of a finite number of monochromatic wave trains of different frequencies. Then

$$S_{\eta\eta}(\omega) = \sum_{i=1}^N \frac{H_i^2}{16} \{ \delta(\omega - \omega_i) + \delta(\omega + \omega_i) \}, \tag{76}$$

where  $\delta(\cdot)$  denotes Dirac delta function,  $\omega_i$  and  $H_i$  represent, respectively, the wave frequency and the wave height of the  $i$ th wave train, and are given by

$$\omega_i = i\Delta\omega \tag{77a}$$

$$H_i = 4\sqrt{S_{\eta\eta}(\omega_i) \Delta\hat{\omega}}, \tag{77b}$$

in which  $\Delta\omega$  is a suitable frequency band width,  $S_{\eta\eta}(\omega_i)$  the ordinate of the original incident wave spectrum at frequency  $\omega_i$ , and  $\Delta\hat{\omega}$  a small frequency band width (which may or may not be made equal to  $\Delta\omega$ ). Equation (77b) is based on the premise that the energy of random waves within a very small frequency band centered at  $\omega_i$  is equivalent to that of a monochromatic wave train of that frequency. Substituting the discretized form of the wave spectrum given in Equation (76) for the wave spectra in Equation (74) results in

$$\begin{aligned} S_{F_x^{(2)} F_x^{(2)}}(\lambda) &= \left( \frac{ag\phi\pi}{2} \right)^2 \int_{-\infty}^{\infty} \sum_{i=1}^N \sum_{j=1}^N \frac{H_i^2 H_j^2}{16^2} \sum_{m=0}^{\infty} \sum_{n=0}^{\infty} \Psi_{m,n}(\omega, \lambda - \omega, a) \{ \delta(\omega - \omega_i) \delta(\lambda - \omega - \omega_j) \\ &\quad + \delta(\omega - \omega_i) \delta(\lambda - \omega + \omega_j) + \delta(\omega + \omega_i) \delta(\lambda - \omega - \omega_j) + \delta(\omega + \omega_i) \delta(\lambda - \omega + \omega_j) \} d\omega \\ &= \sum_{i=1}^N \sum_{j=1}^N \frac{H_i^2 H_j^2}{16^2} \sum_{m=0}^{\infty} \sum_{n=0}^{\infty} \{ \Psi_{m,n}(\omega_i, \lambda - \omega_i, a) \delta(\lambda - \omega_i - \omega_j) + \Psi_{m,n}(\omega_i, \lambda - \omega_i, a) \\ &\quad \cdot \delta(\lambda - \omega_i + \omega_j) + \Psi_{m,n}(-\omega_i, \lambda + \omega_i, a) \delta(\lambda + \omega_i - \omega_j) \\ &\quad + \Psi_{m,n}(-\omega_i, \lambda + \omega_i, a) \delta(\lambda + \omega_i + \omega_j) \}, \end{aligned} \tag{78}$$

where  $\Psi_{m,n}(\dots)$  denotes the square-bracketed term in Equation (74), consisting of the

interaction kernels,  $K_m(\dots)$ ,  $K_n(\dots)$ ,  $L_m(\dots)$  and  $L_n(\dots)$ . By substituting  $p\Delta\omega$ , where  $p$  is an integer, for  $\lambda$  in Equation (78), the power spectral density can be expressed as

$$\begin{aligned}
 S_{F_x^{(2)} F_x^{(2)}}(p\Delta\omega) = & \left(\frac{ag\rho\pi}{2}\right)^2 \left\{ \sum_{\substack{i=1 \\ \text{with}}}^N \sum_{\substack{j=1 \\ i+j=p}}^N \frac{H_i^2 H_j^2}{16^2} \sum_{m=0}^{\infty} \sum_{n=0}^{\infty} \Psi_{m,n}(i\Delta\omega, j\Delta\omega, a) \right. \\
 & + \sum_{\substack{i=1 \\ \text{with}}}^N \sum_{\substack{j=1 \\ i-j=p}}^N \frac{H_i^2 H_j^2}{16^2} \sum_{m=0}^{\infty} \sum_{n=0}^{\infty} \Psi_{m,n}(i\Delta\omega, -j\Delta\omega, a) \\
 & + \sum_{\substack{i=1 \\ \text{with}}}^N \sum_{\substack{j=1 \\ j-i=p}}^N \frac{H_i^2 H_j^2}{16^2} \sum_{m=0}^{\infty} \sum_{n=0}^{\infty} \Psi_{m,n}(-i\Delta\omega, j\Delta\omega, a) \\
 & \left. + \sum_{\substack{i=1 \\ \text{with}}}^N \sum_{\substack{j=1 \\ i+j=-p}}^N \frac{H_i^2 H_j^2}{16^2} \sum_{m=0}^{\infty} \sum_{n=0}^{\infty} \Psi_{m,n}(-i\Delta\omega, -j\Delta\omega, a) \right\}. \quad (79)
 \end{aligned}$$

It is noted that the power spectral density represented by Equation (79) takes nonzero values at discrete frequencies only. Utilizing Equation (63), it can be shown that

$$\Psi_{m,n}(i\Delta\omega, -j\Delta\omega, a) = \Psi_{m,n}(-i\Delta\omega, j\Delta\omega, a), \quad (80)$$

and, therefore, the power spectral density in Equation (79) may be rewritten as

$$\begin{aligned}
 S_{F_x^{(2)} F_x^{(2)}}(p\Delta\omega) = & \left(\frac{ag\rho\pi}{2}\right)^2 \left\{ \sum_{\substack{i=1 \\ \text{with}}}^N \sum_{\substack{j=1 \\ i+j=p}}^N \frac{H_i^2 H_j^2}{16^2} \sum_{m=0}^{\infty} \sum_{n=0}^{\infty} \Psi_{m,n}(i\Delta\omega, j\Delta\omega, a) \right. \\
 & + \sum_{\substack{i=1 \\ \text{with}}}^N \sum_{\substack{j=1 \\ i-j=p}}^N \frac{H_i^2 H_j^2}{16^2} \sum_{m=0}^{\infty} \sum_{n=0}^{\infty} 2\Psi_{m,n}(i\Delta\omega, -j\Delta\omega, a) \\
 & \left. + \sum_{\substack{i=1 \\ \text{with}}}^N \sum_{\substack{j=1 \\ j-i=p}}^N \frac{H_i^2 H_j^2}{16^2} \sum_{m=0}^{\infty} \sum_{n=0}^{\infty} \Psi_{m,n}(-i\Delta\omega, -j\Delta\omega, a) \right\}. \quad (81)
 \end{aligned}$$

It is noted from Equation (81) that the first term (for  $p > 0$ ) or the third term (for  $p < 0$ ) provides the spectral value at the sum frequency of the interacting wave components, and the second term the spectral value at the difference frequency of the interacting wave components. It is apparent that the evaluation of  $\Psi_{m,n}(\dots)$  in Equation (81) represents the major computational task in obtaining the power spectral density of the second-order diffraction forces. Based on the discretization scheme of the wave spectrum described above, computations are carried out for some numerical examples to demonstrate the spectral content of the first-order and second-order diffraction forces. It is worth pointing out at this point that although Equation (81) provides spectral values of the second-order diffraction forces only at various discrete frequencies (as a result of the discretization of the incident wave spectrum), many features of the power spectral density of the second-order diffraction forces can still be observed. By

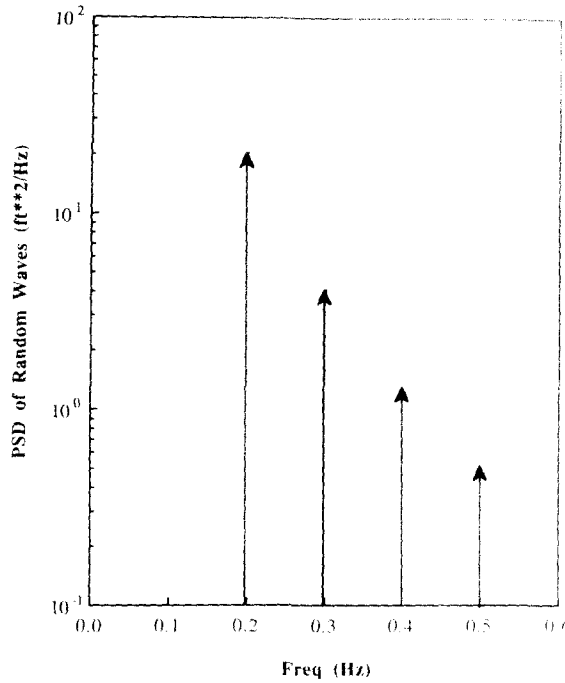


FIG. 2. Power spectral density of an incident wave field consisting of waves at 0.2, 0.3, 0.4 and 0.5 Hz.

increasing the number of discrete wave components, a finer resolution of the power spectral density of the second-order diffraction forces may be obtained.

As the  $r$ -integral included in the double integral  $L_q(\dots)$  defined in Equation (62b) has a highly oscillatory integrand, special consideration has to be given to the numerical integration of this term. Herein, the numerical evaluation of  $r$ -integral is carried out in a way similar to that applied by Hunt and Baddour (1981) and Hunt and Williams (1982). Thus, three terms of the asymptotic behavior of  $C_1(kr)C_q(k_1r)C_{q+1}(k_2r)$  are subtracted from the integrand, integrated by parts, and evaluated explicitly in terms of Fresnel integrals. The remaining integral, which tends to zero monotonically as  $r$  approaches infinity, is then evaluated by a series of Gaussian quadratures over an interval  $[a,R]$  where  $R/a$  is large but finite, and  $R$  depends on the values of  $k, k_1, k_2,$  and  $q$ . For  $k_1 \neq k_2$ , the  $r$ -integration results in two weak singularities in the  $k$ -integrand. One weak singularity, which behaves as  $|k - (k_1 + k_2)|^{-1/2}$  near  $k = k_1 + k_2$ , is removed by the factor  $[k^2 - (k_1 + k_2)^2]$  in the  $k$ -integrand; the other, which behaves as  $|k - |k_1 - k_2||^{-1/2}$  near  $k = |k_1 - k_2|$ , is integrable by a change of variables in the integrand. For  $k_1 = k_2$ , the two weak singularities are reduced to one, which behaves as  $|k - 2k_1|^{-1/2}$  near  $k = 2k_1$ , which was removable as reported previously by Hunt and Baddour (1981) and Hunt and Williams (1982). For the  $k$ -integral, a singularity also occurs at  $k = k_s = (\omega_1 + \omega_2)^2/g$ . Near  $k = k_s$ , the integrand behaves as  $|k - k_s|^{-1}$  and results in a Cauchy principal value.

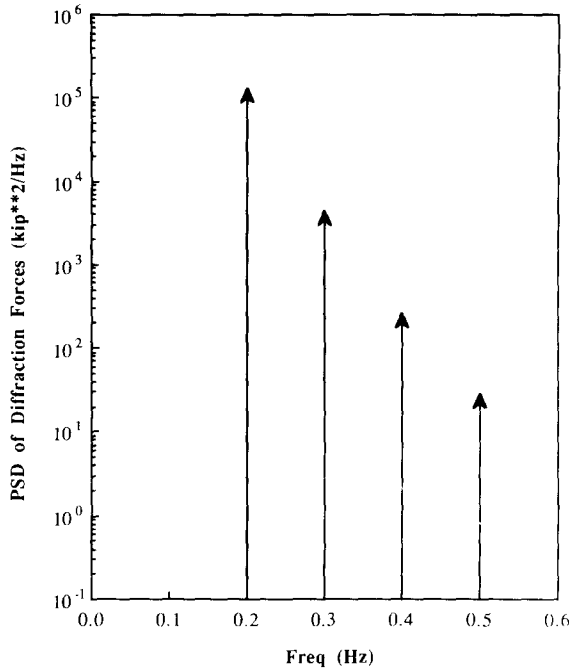


FIG. 3. Power spectral density of the first-order diffraction forces due to an incident wave field consisting of waves at 0.2, 0.3, 0.4 and 0.5 Hz.

NUMERICAL RESULTS AND DISCUSSIONS

An example vertical circular cylinder having a diameter of 30 ft is selected for the numerical computations, and the incident wave spectrum is represented by a superposition of band-limited white noise processes, as given in Equation (76), centered at frequencies greater than or equal to 0.2 Hz, for which wave diffraction becomes increasingly significant. The value of  $\Delta\omega$  in Equation (77a) is chosen equal to 0.1 Hz. The incident wave spectral amplitude is determined from Equation (77b) based on the condition that each wave train has a wave steepness of 0.1 and  $\Delta\hat{\omega} = 0.0628$  rad/sec ( $= 2\pi \times 0.01$  Hz); therefore

$$\begin{aligned}
 S_{\eta\eta}(2\pi f_i) &= \frac{H_i^2}{16 \times 0.0628} \\
 &= \frac{(0.1 L_i)^2}{16 \times 0.0628}
 \end{aligned}
 \tag{82}$$

where  $H_i$  and  $L_i$  denote, respectively, the wave height and wave length of a monochromatic wave train of wave frequency  $f_i$ , and  $L_i$  can be obtained from the linear deepwater dispersion relation. For convenience, in the following the spectral figures are one-sided and the wave frequency in the figures is given in hertz.

Figure 2 presents the spectral representation of an incident wave field consisting of four dominant wave components of 0.2, 0.3, 0.4 and 0.5 Hz, based on Equation (82). Figure 3 illustrates the spectral description of the first-order diffraction forces in such

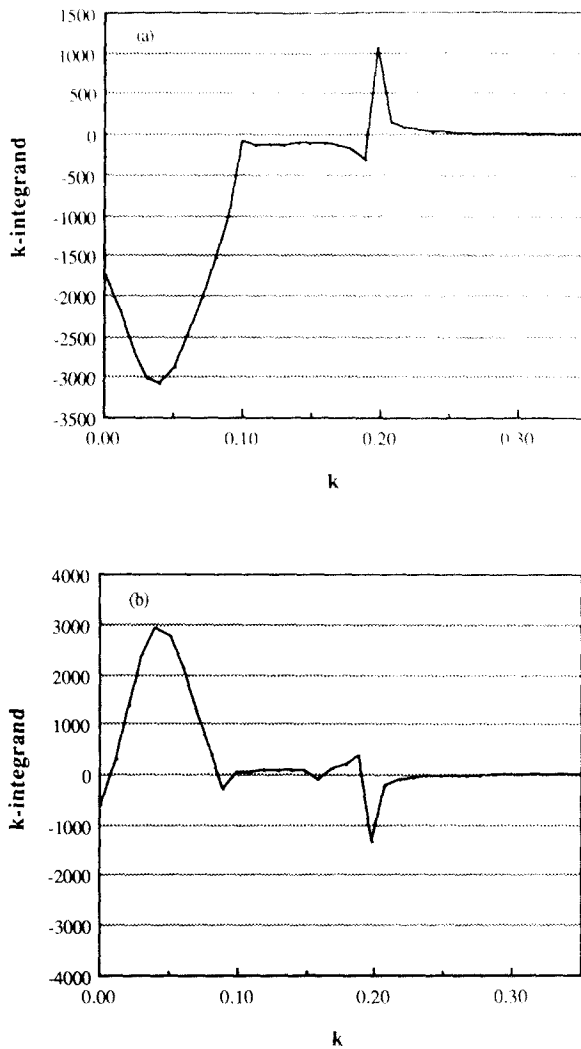


FIG. 4.  $k$ -integrand at double frequency corresponding to an individual wave at 0.2 Hz (a) order 0; (b) order 1.

a random wave field. Several results for the power spectral density of the second-order diffraction loading may be obtained by taking combinations (two, three or four, respectively) of the incident wave spectral amplitudes shown in Fig. 2.

In obtaining the spectral content of the second-order diffraction forces, the infinite summation in Equation (81) was truncated after a finite number of terms. This number was determined by numerical testing so as to ensure that the computed results were accurate to two significant digits. Generally, more terms are required for the spectral contribution introduced by self-interaction of the individual wave components than that for the spectral components contributed by interactions between wave components at different frequencies. In addition, among the spectral contributions due to interactions

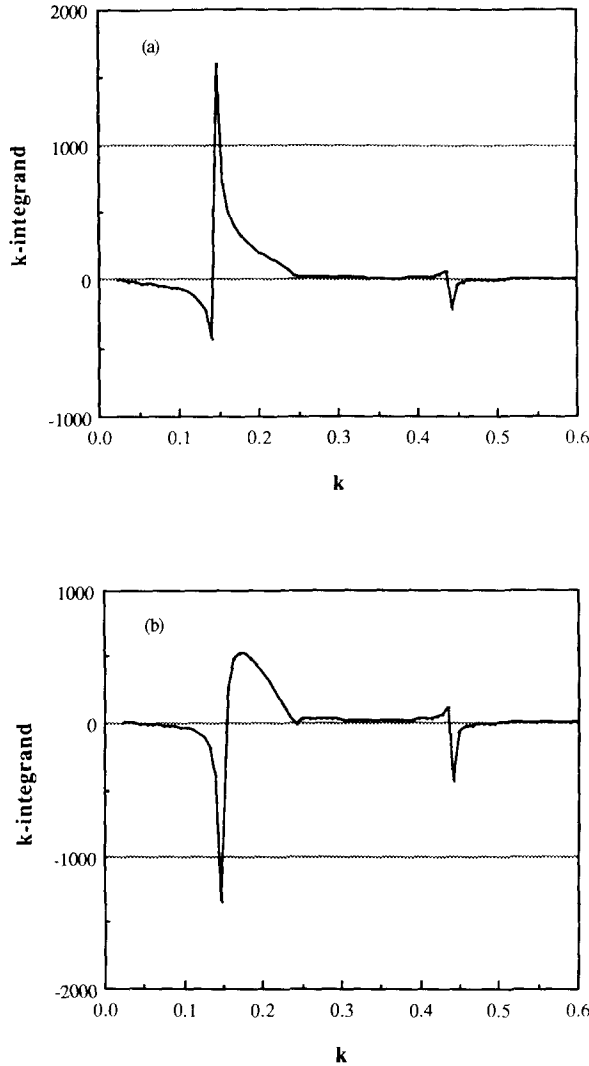


FIG. 5.  $k$ -integrand at sum frequency corresponding to a wave pair at 0.2 and 0.4 Hz (a) order 0; (b) order 1.

between wave components at different frequencies, the number of terms required to compute interactions between two waves at relatively close frequencies is larger than that required for two wave components with a large difference in their frequencies.

A progressively finer mesh of Gaussian points with increasing  $q$  in the  $r$ -integration is applied to ensure monotonic decrease in the  $k$ -integrand as the value of  $k$  increases (Hunt and Williams, 1982). Typical  $k$ -integrands for the first two orders (0 and 1) corresponding to different wave frequency conditions are illustrated in Figs 4(a)–6(b). Figure 4(a) and (b) presents profiles of the  $k$ -integrand at a double frequency corresponding to an individual wave at 0.2 Hz. It is noted that there is a singularity at  $k = 0.19651$ , which results in a Cauchy principal value, and the  $k$ -integrand decreases

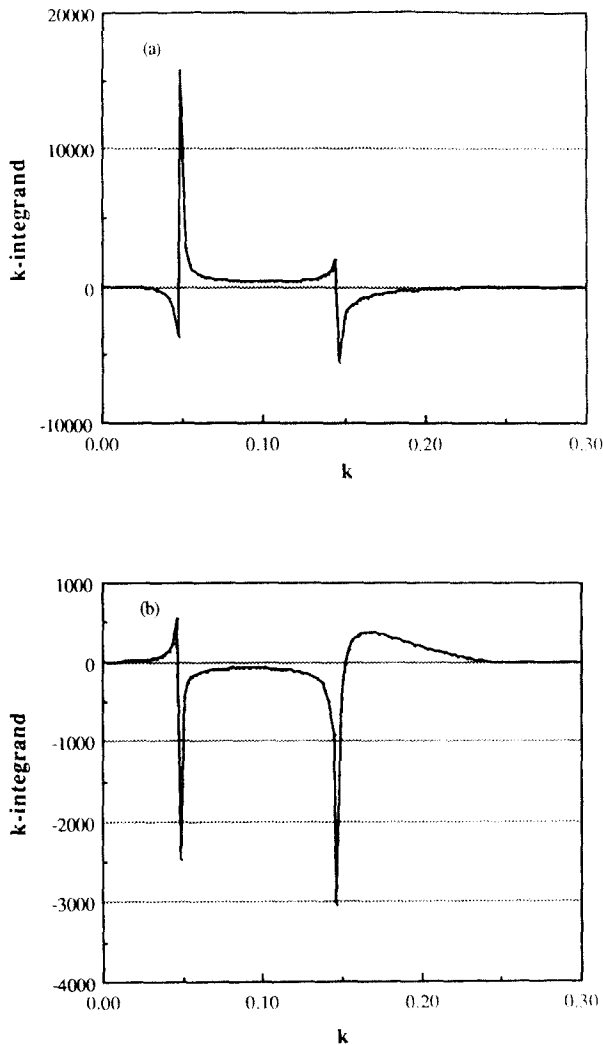


FIG. 6.  $k$ -integrand at difference frequency corresponding to a wave pair at 0.2 and 0.4 Hz (a) order 0; (b) order 1.

rapidly for larger values of  $k$ . Figure 5(a) and (b) presents the  $k$ -integrand at a sum frequency corresponding to a wave pair at 0.2 and 0.4 Hz. It can be seen from the figures that a weak singularity occurs at  $k = 0.14734$ , and a further singularity is present at  $k = 0.44203$ . Figure 6(a) and (b) presents the  $k$ -integrand at a difference frequency corresponding to a wave pair at 0.2 and 0.4 Hz. A singularity is present at  $k = 0.04911$  and a weak singularity exists at  $k = 0.14734$ . The numerical integration for the  $k$ -integral in the present work was carried out by use of Gaussian quadrature. From the figures, it can be seen that the value of the  $k$ -integrand is negligible at large values of  $k$ . Extensive numerical testing has showed that when  $k_1 = k_2$  (the case of double frequency), the major contribution results from values of  $k < k_s$ ; when  $k_1 \neq k_2$ , the

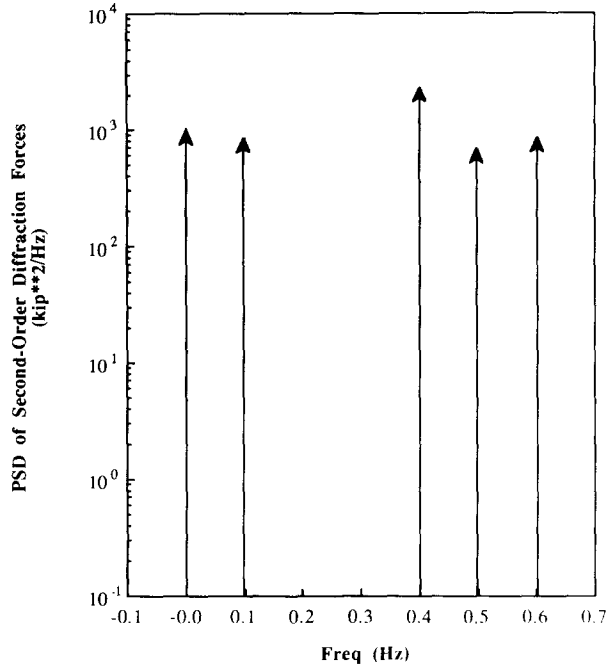


FIG. 7. Power spectral density of the second-order diffraction forces due to an incident wave field consisting of waves at 0.2 and 0.3 Hz.

major contribution results from values of  $k < 1.5k_s$  for the case of  $k_s > |k_1 - k_2|$  (the case of sum frequency), and from values of  $k < 2|k_1 - k_2|$  for the case of  $k_s < |k_1 - k_2|$  (the case of difference frequency). These values may be used as guidelines to specify a finite  $k$ -interval in any future work.

Figure 7 presents the spectral representation of the second-order diffraction forces resulting from an incident wave field at two wave frequencies, 0.2 and 0.3 Hz. It is noted from the figure that spectral contributions occur, as a result of self-interaction of individual random waves, at zero and double frequencies (i.e. at 0.0, 0.4 and 0.6 Hz), and as a result of interaction between random waves of different frequencies, at 0.1 Hz (difference frequency) and 0.5 Hz (sum frequency). The spectral value at 0.1 Hz is about 83% of that at 0.0 Hz and the spectral amplitude at 0.5 Hz is about 80% of that at 0.6 Hz, indicating that the spectral contribution from the interaction of waves of different frequencies can be significant. Figure 8 shows spectral amplitudes of the second-order diffraction forces in a wave field consisting of three random waves of 0.2, 0.3 and 0.4 Hz. In comparison with the previous case (Fig. 8), it is noticed that as a consequence of interaction between random waves of 0.3 and 0.4 Hz, the spectral amplitude at 0.1 Hz (difference frequency) has an increase of approximately 4% and a new spectral contribution appears at 0.7 Hz (sum frequency). In addition, due to the interaction between random waves of 0.2 and 0.4 Hz, the spectral ordinate at 0.6 Hz (sum frequency) is increased again by approximately 4% and a new spectral contribution occurs at 0.2 Hz (difference frequency). It is also observed that at either sum or difference frequency, the interaction between random waves of 0.3 and 0.4 Hz

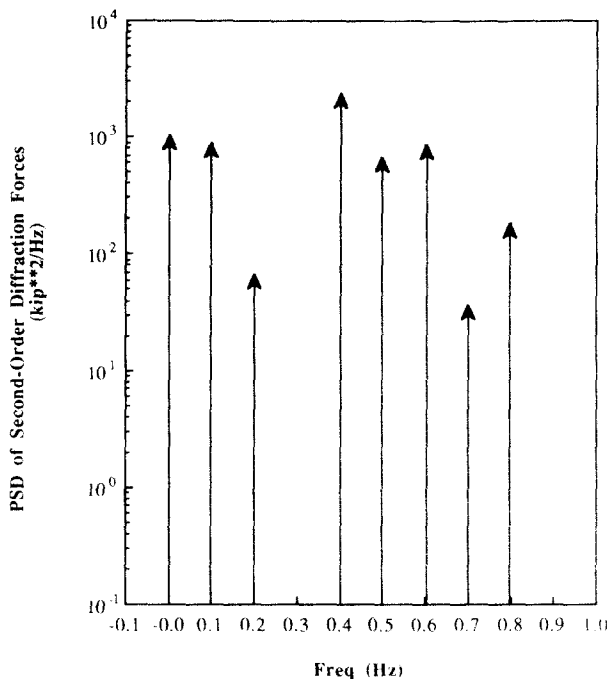


FIG. 8. Power spectral density of the second-order diffraction forces due to an incident wave field consisting of waves at 0.2, 0.3 and 0.4 Hz.

gives rise to a smaller spectral impulse than does that of 0.2 and 0.3 Hz, which can be attributed to the fact that the incident wave spectral amplitude at 0.4 Hz is only 6% of that of 0.2 Hz. Moreover, it is found that spectral amplitude at sum and difference frequencies arising from wave frequencies of 0.2 and 0.3 Hz are, respectively, 21.7 and 12.5 times greater than those at the sum and difference frequencies arising from waves at 0.2 and 0.4 Hz although the incident wave spectral amplitude at 0.3 Hz is no more than 3.2 times greater than that at 0.4 Hz. This suggests that the greater the frequency difference between the two wave components, the less intense is the interaction between them.

The above-stated trend can be confirmed by considering the case of an incident wave field consisting of four wave components, as shown in Fig. 2. Figure 9 presents the spectral description of the second-order diffraction loading in such an incident wave field. It is noted that interactions between the wave pair at 0.2 and 0.5 Hz result in a spectral contribution at 0.3 Hz (difference frequency) and a 14.5% increase in the spectral value at 0.7 Hz (sum frequency). Also, it is found that the spectral contributions at the sum and difference frequencies by the wave pair at 0.2 and 0.4 Hz are, respectively, 5.7 and 125.3 times greater than those induced at the sum and difference frequencies by the wave pair at 0.2 and 0.5 Hz although the incident wave spectral impulse at 0.4 Hz is only 2.4 times greater than that at 0.5 Hz. Aside from the interaction of waves at different frequencies, the results from Figs 3 and 9 suggest that the intensity of the self-interaction of the individual wave components increases with increasing wave frequency, as evidenced by the ratio of the spectral amplitude of the

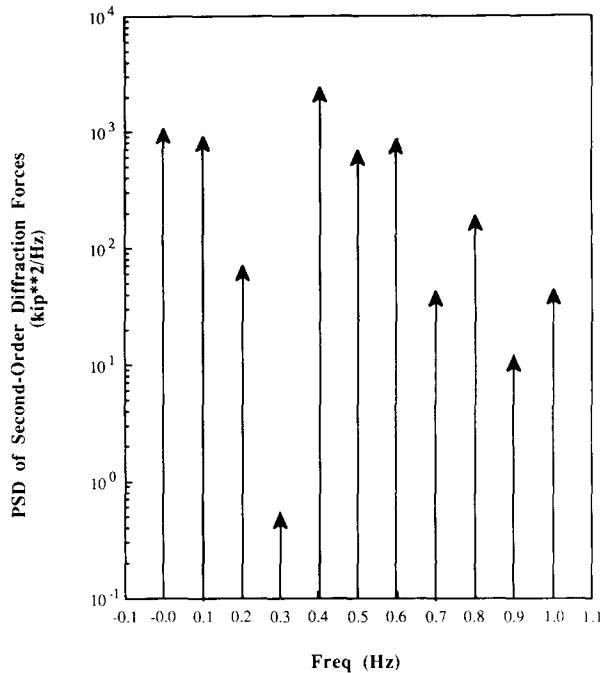


FIG. 9. Power spectral density of the second-order diffraction forces due to an incident wave field consisting of waves at 0.2, 0.3, 0.4 and 0.5 Hz.

second-order diffraction forces at the double frequency to that of the first-order diffraction forces at the incident wave frequency. This ratio rises from 1.8 to 18.4 to 71.4% and finally to 153.3% as the incident wave frequency varies from 0.2 to 0.5 Hz in 0.1 Hz increments. It is also noted from Figs 3 and 9 that the spectral amplitudes of the second-order diffraction forces at 0.4 and 0.5 Hz are about 9 times greater and 23 times greater, respectively, than that of the first-order diffraction forces at the corresponding frequencies, and the spectral impulses of the second-order diffraction force at frequencies higher than 0.5 Hz are greater or comparable to that of the first-order force at 0.5 Hz, emphasizing the significance of second-order effects in shaping the spectral content of the nonlinear diffraction force in the high frequency range.

#### CONCLUDING REMARKS

A theory of nonlinear diffraction of random waves by a vertical uniform circular cylinder in deep water has been presented, with emphasis on the spectral description of the second-order diffraction forces. From the numerical results shown herein, it is clear that the spectral density of the second-order diffraction forces in a random incident wave field is influenced not only by the self-interactions of the individual wave components, but also by the interactions between the different wave components. The present approach provides a complete spectral description of the second-order diffraction forces, and illustrates the significance of wave-wave interactions in yielding spectral densities at the sum and difference frequencies.

*Acknowledgements*—Support for this study was provided in part by the National Science Foundation (grant Nos BCS-90-96279 and BCS-835223) and the Texas Advanced Technology Program (grant No. 2022-ATP). This support is gratefully acknowledged.

## REFERENCES

- ABUL-AZM, A.G. and WILLIAMS, A.N. 1988. Second-order diffraction loads on truncated cylinders. *J. WatWay, Port, Coastal Ocean Div., ASCE* **114**, 436–454.
- ABUL-AZM, A.G. and WILLIAMS, A.N. 1989a. Approximation of second-order diffraction loads on vertical cylinder arrays. *J. Fluids Struct.* **3**, 17–36.
- ABUL-AZM, A.G. and WILLIAMS, A.N. 1989b. Second-order diffraction loads on arrays of semi-immersed cylinders. *J. Fluids Struct.* **3**, 365–388.
- DOOB, J.L. 1953. *Stochastic Processes*. John Wiley and Sons, New York.
- EATOCK TAYLOR, R. and CHAU, F.P. 1992. Wave diffraction theory—some developments in linear and nonlinear theory. *J. Offshore Mech. Arctic Engng, ASME* **114**, 185–194.
- EATOCK TAYLOR, R.E. and HUNG, S.M. 1987. Second-order diffraction forces on a vertical cylinder in regular waves. *Appl. Ocean Res.* **9**, 19–30.
- GHALAYINI, S.A. and WILLIAMS, A.N. 1989. Nonlinear wave forces on vertical cylinders of arbitrary cross-section. *J. WatWay, Port, Coastal Ocean Div., ASCE* **115**, 809–830.
- GHALAYINI, S.A. and WILLIAMS, A.N. 1991. Nonlinear wave forces on vertical cylinder arrays. *J. Fluids Struct.* **5**, 1–32.
- GRIFFITH, J.L. 1956. On Weber transforms. *Proc. Roy. Soc. New South Wales* **90**, 232.
- GRIFFITH, J.L. 1957. A note on a generalization of Weber's Transform. *Proc. Roy. Soc. New South Wales* **89**, 157.
- HAVELOCK, T.H. 1940. The pressure of water waves upon a fixed obstacle. *Proc. Roy. Soc. London, A* **175**, 409–421.
- HUNT, J.N. and BADDOUR, R.E. 1981. The diffraction of nonlinear progressive waves by a vertical cylinder. *Q. J. Mech. appl. Math.* **34**, 69–87.
- HUNT, J.N. and WILLIAMS, A.N. 1982. Nonlinear diffraction of Stokes water waves by a circular cylinder for arbitrary uniform depth. *J. Mecanique Theorique Appliquee* **1**, 429–449.
- KIM, M.H. 1991. Second-order sum-frequency wave loads on large-volume structures. *Appl. Ocean Res.* **13**, 287–296.
- KIM, M.H. and YUE, D.K.P. 1989. The complete second-order solution for an axisymmetric body. Part 1: monochromatic incident waves. *J. Fluid Mech.* **200**, 235–264.
- KIM, M.H. and YUE, D.K.P. 1990. The complete second-order solution for an axisymmetric body. Part 2: bichromatic incident waves and body motions. *J. Fluid Mech.* **211**, 557–593.
- KIM, M.H. and YUE, D.K.P. 1991. Sum- and difference-frequency wave loads on a body in unidirectional Gaussian seas. *J. Ship Res.* **35**, 127–140.
- LIGHTHILL, M.J. 1979. Waves and hydrodynamic loading. *Behavior of Offshore Structures Conference BOSS '79, London, U.K.*, pp. 1–40.
- MACCAMY, R.C. and FUCHS, R.A. 1954. Wave forces on piles: a diffraction theory. Technical Memorandum No. 69, U.S. Beach Erosion Board.
- MOLIN, B. 1979. Second-order diffraction loads on three-dimensional bodies. *Appl. Ocean Res.* **1**, 197–202.
- WATSON, G.N. 1952. *A Treatise on the Theory of Bessel Functions*. Cambridge University Press, Cambridge.
- WILLIAMS, A.N. 1989. Nonlinear diffraction effects on tension-leg platforms. *The Tension-leg Platform: a State-of-the-Art Review*, DEMIRBILEK, Z. (ed.), ASCE monograph, pp. 227–260.
- YAGLOM, A.M. 1962. *An Introduction to the Theory of Stationary Random Functions*. Prentice-Hall, Englewood Cliffs.

## APPENDIX

In this appendix the total second-order velocity potential will be shown to satisfy Laplace's equation and two boundary conditions prescribed in Equations (14)–(16). Formally, the total second-order velocity potential can be expressed as

$$\Phi^{(2)}(r, \theta, z, t) = \int_{-\infty}^{\infty} \int_{-\infty}^{\infty} \sum_{n=-\infty}^{\infty} \sum_{m=-\infty}^{\infty} A_{n,m}(\Omega, k) C_n(kr) e^{ikz} e^{im\theta} e^{i\Omega t} dk d\xi_2(\Omega). \quad (A1)$$

From the following identities

$$J_n(-x) = (-1)^n J_n(x) \quad \text{and} \quad Y_n(-x) = (-1)^n [Y_n(x) + i2J_n(x)], \quad (A2)$$

valid for  $x > 0$ , it follows that for  $k > 0$ ,

$$C_n(-kr) = -C_n(kr). \quad (\text{A3})$$

Therefore, the  $k$ -integral in Equation (A1) can be expressed as

$$\begin{aligned} \int_{-\infty}^{\infty} A_{n,m}(\Omega, k) C_n(kr) e^{k|z} dk &= \int_0^{\infty} A_{n,m}(\Omega, k) C_n(kr) e^{kz} dk + \int_{-\infty}^0 A_{n,m}(\Omega, k) C_n(kr) e^{-kz} dk \\ &= \int_0^{\infty} A_{n,m}(\Omega, k) C_n(kr) e^{kz} dk + \int_0^{\infty} A_{n,m}(\Omega, -k) C_n(-kr) e^{kz} dk \\ &= \int_0^{\infty} G_{n,m}(\Omega, k) C_n(kr) e^{kz} dk, \end{aligned} \quad (\text{A4})$$

where

$$G_{n,m}(\Omega, k) = A_{n,m}(\Omega, k) - A_{n,m}(\Omega, -k). \quad (\text{A5})$$

Subsequently,  $\Phi^{(2)}$  can be written as

$$\Phi^{(2)}(r, \theta, z, t) = \int_{-\infty}^{\infty} \int_0^{\infty} \sum_{n=-\infty}^{\infty} \sum_{m=-\infty}^{\infty} G_{n,m}(\Omega, k) C_n(kr) e^{kz} e^{in\theta} e^{i\Omega t} dk d\xi_2(\Omega). \quad (\text{A6})$$

It can be proven that this form for  $\Phi^{(2)}$  satisfies Laplace's equation. Let  $h_{n,m}(r, \theta, z, k)$  be defined as follows:

$$h_{n,m}(r, \theta, z, k) = C_n(kr) e^{kz} e^{in\theta}. \quad (\text{A7})$$

Substitution of  $h_{n,m}(r, \theta, z, k)$  into the Laplacian operator in cylindrical coordinate system leads to

$$\nabla^2 h_{n,m}(r, \theta, z, k) = \left\{ k^2 C_n''(kr) + \frac{k}{r} C_n'(kr) - \frac{n^2}{r^2} C_n(kr) + k^2 C_n(kr) \right\} e^{kz} e^{in\theta}. \quad (\text{A8})$$

Since the Bessel functions satisfy the following recurrence relations [see, for example, Watson (1952)],

$$D_{\nu-1}(z) + D_{\nu+1}(z) = \frac{2\nu}{z} D_{\nu}(z),$$

$$D_{\nu-1}(z) - D_{\nu+1}(z) = 2D_{\nu}'(z) \quad \text{and}$$

$$D_{\nu-2}(z) - 2D_{\nu}(z) + D_{\nu+2}(z) = 4D_{\nu}''(z), \quad (\text{A9})$$

where  $D_{\nu}(z)$  denotes the cylinder function, it follows that

$$\begin{aligned} k^2 C_n''(kr) &= k^2 \left\{ Y_n'(ka) \left[ \frac{1}{4} J_{n-2}(kr) - \frac{1}{2} J_n(kr) + \frac{1}{4} J_{n+2}(kr) \right] \right. \\ &\quad \left. - J_n'(ka) \left[ \frac{1}{4} Y_{n-2}(kr) - \frac{1}{2} Y_n(kr) + \frac{1}{4} Y_{n+2}(kr) \right] \right\}, \end{aligned} \quad (\text{A10a})$$

$$\begin{aligned} \frac{k}{r} C_n'(kr) &= \frac{k^2}{4(n-1)} \left\{ Y_n'(ka) [J_{n-2}(kr) + J_n(kr)] - J_n'(ka) [Y_{n-2}(kr) + Y_n(kr)] \right\} \\ &\quad + \frac{k^2}{4(n+1)} \left\{ J_n'(ka) [Y_n(kr) + Y_{n+2}(kr)] - Y_n'(ka) [J_n(kr) + J_{n+2}(kr)] \right\}, \end{aligned} \quad (\text{A10b})$$

$$\begin{aligned} -\frac{n^2}{r^2} C_n(kr) &= \frac{nk^2}{4(n-1)} \left\{ J_n'(ka) [Y_{n-2}(kr) + Y_n(kr)] - Y_n'(ka) [J_{n-2}(kr) + J_n(kr)] \right\} \\ &\quad + \frac{nk^2}{4(n+1)} \left\{ J_n'(ka) [Y_{n+2}(kr) + Y_n(kr)] - Y_n'(ka) [J_{n+2}(kr) + J_n(kr)] \right\} \end{aligned} \quad (\text{A10c})$$

and

$$k^2 C_n(kr) = k^2 [Y_n'(ka) J_n(kr) - J_n'(ka) Y_n(kr)]. \quad (\text{A10d})$$

Summing Equations (A10a)–(A10d) leads to

$$\begin{aligned}
 k^2 C_n''(kr) + \frac{k}{r} C_n'(kr) - \frac{n^2}{r^2} C_n(kr) + k^2 C_n(kr) &= \left[ \frac{k^2}{4} + \frac{k^2}{4(n-1)} - \frac{nk^2}{4(n-1)} \right] \\
 \cdot \{ Y_n'(ka) J_{n-2}(kr) - J_n'(ka) Y_{n-2}(kr) \} &+ \left[ -\frac{k^2}{2} + \frac{k^2}{4(n-1)} - \frac{k^2}{4(n+1)} - \frac{nk^2}{4(n-1)} - \frac{nk^2}{4(n+1)} + k^2 \right] \\
 \cdot \{ Y_n'(ka) J_n(kr) - J_n'(ka) Y_n(kr) \} &+ \left[ \frac{k^2}{4} - \frac{k^2}{4(n+1)} - \frac{nk^2}{4(n+1)} \right] \\
 \cdot \{ Y_n'(ka) J_{n+2}(kr) - J_n'(ka) Y_{n+2}(kr) \}. & \tag{A11}
 \end{aligned}$$

It is noted that each of the coefficients (in square brackets) in Equation (A11) is identically zero. Therefore, it can be concluded from Equations (A6) to (A8) and (A11) that

$$\nabla^2 \Phi^{(2)}(r, \theta, z, t) = 0. \tag{A12}$$

Furthermore, since

$$\left. \frac{\partial C_n(kr)}{\partial r} \right|_{r=a} = k \{ Y_n'(ka) J_n'(kr) - J_n'(ka) Y_n'(kr) \} \Big|_{r=a} = 0.$$

it follows that

$$\left. \frac{\partial \Phi^{(2)}(r, \theta, z, t)}{\partial r} \right|_{r=a} = 0. \tag{A13}$$

Finally, from Equation (A6), since  $\Phi^{(2)}$  contains the depth-decay factor  $e^{kz}$ ,

$$\left. \frac{\partial \Phi^{(2)}(r, \theta, z, t)}{\partial z} \right|_{z=0} \rightarrow 0 \quad \text{as } z \rightarrow -\infty. \tag{A14}$$